Geothermics 70 (2017) 393–405

Contents lists available at ScienceDirect

Geothermics

journal homepage: www.elsevier.com/locate/geothermics

Play fairway analysis of geothermal resources across the state of Hawaii: 2. Resource probability mapping

Garrett Ito[a,*], Neil Frazer[a], Nicole Lautze[b], Donald Thomas[b], Nicholas Hinz[c], David Waller[a], Robert Whittier[d], Erin Wallin[b]

[a] Department of Geology and Geophysics, SOEST, University of Hawaii, Manoa, Honolulu, HI 96822, USA
[b] Hawaiian Institute for Geophysics and Planetology, SOEST, University of Hawaii, Manoa, Honolulu, HI 96822, USA
[c] Nevada Bureau of Mines and Geology, Mackay School of Earth Sciences and Engineering, University of Nevada, Reno, USA
[d] Safe Drinking Water Branch, Hawaii State Department of Health, USA

ARTICLE INFO

Article history:
Received 28 May 2016
Received in revised form 7 October 2016
Accepted 4 November 2016
Available online 15 December 2016

Keywords:
Volcanic islands
Resource prospecting
Data analysis
Geology
Geophysics
Geochemistry
Probability and statistics

ABSTRACT

We develop a new geostatistical method to combine evidence provided by diverse geological data sets and produce maps of geothermal resource probability. The application is to the State of Hawaii, and the data sets include the locations and ages of mapped volcanic centers, gravity and magnetotelluric measurements, groundwater temperature and geochemistry, ground surface deformation, seismicity, water table elevation, and groundwater recharge. Using the basic principles of Bayesian statistics, these data and expert knowledge about the effects and importance of the data are used to compute the probabilities of the primary resource qualities of elevated subsurface heat, reservoir permeability, and reservoir fluid content. The product of these marginal probabilities estimates the joint probability of all three qualities and hence the probability of a successful geothermal prospect at each map point. An analogous set of algorithms is used to quantify the confidence in the probability at each point. Not surprisingly, we find that successful geothermal prospects are most probable on the active volcanoes of Hawaii Island, including the area of Hawaii's single geothermal energy plant. Probability decreases primarily with shield volcano age, being relatively moderate in select locations on Maui and Lanai, relatively low on Oahu, and minimal on Kauai. Future exploration efforts should consider these results as well as the practical, societal, and economic conditions that influence development viability. The difficulties of interisland power transmission mean that even areas with moderate to low probabilities are worth investigating on islands with population centers.

1. Introduction

We conducted an assessment of geothermal resource potential across the state of Hawaii, updating the last assessment which was done three decades ago (Thomas, 1985). The overall goal is to identify the *plays*, or probable areas for geothermal energy development in the *fairway*, of the Hawaiian volcanic island chain. The first of three manuscripts (Lautze et al., 2016a) summarizes the geologic conditions that support geothermal resources in Hawaii and the datasets selected to provide evidence for these conditions. The third paper (Lautze et al., 2016b) describes the essential practical and economic criteria needed to assess *development viability* and, with the results of the geologic considerations presented in this paper, recommends a prioritized list of sites for future exploration. This manuscript—the second paper in the series—describes our methods and the results of processing the various geoscientific datasets into probabilities of geothermal resources across the state.

Methods used to map the spatial distributions of geothermal resource potential can be categorized as knowledge-driven or data-driven (Bonham-Carter, 1994). Knowledge-driven, or deterministic, models rely on the judgment of experts to assign the relative importance of different data types to resource potential. These methods are needed especially in the reconnaissance phase of exploration when few or no resources have been found (e.g. Prol-Ledesma, 2000). Techniques of combining the evidence provided by the data include Boolean operators (Noorollahi et al., 2008; Yousefi et al., 2010), index quantification and weighting (Noorollahi et al., 2008; Tüfekçi et al., 2010; Trumpy et al., 2015), and quantification with *fuzzy* or continuous functions (Prol-Ledesma, 2000; Siler et al., 2016). In contrast, data-driven models incorporate *data* on

* Corresponding author.
E-mail address: gito@hawaii.edu (G. Ito).

http://dx.doi.org/10.1016/j.geothermics.2016.11.004
0375-6505/

known resource locations or training sites to relate observational evidence to resource potential. These methods use statistical techniques including weight-of-evidence (Bonham-Carter et al., 1989; Coolbaugh and Bedell, 2006; Coolbaugh et al., 2007), logistic regression (Coolbaugh et al., 2002, 2005), and evidence belief functions (Carranza and Hale, 2003). Data-driven methods have been used even more extensively in mineral resource exploration (e.g., Porwal and Kreuzer, 2010). In this context, the method developed here is knowledge-driven, uses continuous quantities for the influence of different data types, but like some of the data-driven techniques, the core algorithm is based on the principles of Bayesian statistics. Unlike earlier methods used, that produced measures of resource "favorability", our method predicts relative probabilities.

A successful geothermal prospect must have all of three primary qualities: elevated heat (*H*), elevated permeability (*P*), and adequate fluid (*F*) to deliver the heat. Table 1 lists the data types used for Hawaii as indicators of each of quality, and summarizes the evidence each data type provides as discussed in detail by Lautze et al. (2016a). Section 2 of this paper reviews the theory of our method, our approach to eliciting expert knowledge, and the algorithm by which this knowledge and the data are combined to compute probabilities. Section 3 details the specific parameters and functions used for each data type and their individual effects on the marginal probabilities of the three resource qualities. Section 4 presents the resulting resource probabilities and their associated confidence measures for the main Hawaiian Islands. Finally, we close with a discussion of the strengths and weaknesses of our method, and the role our results could play in Hawaii's exploratory decision-making process.

2. Methods of data processing and modeling probability and confidence

2.1. Overview

The first building block of our method is a generalized linear model (e.g., MCullah and Nelder, 1983) in which the evidence provided by each data type is weighted and summed in the logistic link function (e.g., Bonham-Carter et al., 1989),

$$Pr(\mathbf{x}) = \left[1 + \exp\left(-w_0 - \sum_{i=1}^{m} w_i z_i(\mathbf{x})\right)\right]^{-1}. \quad (1)$$

Here $\mathrm{Pr}(\mathbf{x})$ is the probability of just one of the resource qualities (elevated heat *H*, permeability *P*, fluid *F*) at location $\mathbf{x}$ on the map. A similar equation is used for each of the two other qualities. In this equation $z_i(\mathbf{x})$ is a transformed and scaled (explained in Sections 2.2 and 2.3 below), real-number, form of data type *i*; w_i is a weight that reflects the relative importance of data type *i* to the quality of interest; and *m* is the number of data types present at location $\mathbf{x}$. This equation implicitly includes a reference probability, or prior probability Pr_0, represented on the right-hand side by the quantity w_0. We refer to Eq. (1) as the "voter equation" because it allows each data type to influence the outcome (positively or negatively) depending on its weight w_i.

The general behavior of the voter equation can be understood through a qualitative discussion. Suppose z_1 is a quantity representing the gravity anomaly at location $\mathbf{x}$, and z_2 represents a measure of electrical resistivity beneath the ground at $\mathbf{x}$. Because high positive values of gravity are interpreted as indicating dense intrusive source rock (and z_1 is positive when the gravity anomaly is relatively high), the associated weight w_1 will be positive. In contrast, unusually low resistivity (indicated by a negative value of z_2) is associated with hot rock and therefore w_2 will be negative. Thus, a large positive value of the sum $\Sigma = w_0 + w_1 z_1 + w_2 z_2$ indicates a high favorability of elevated heat. Clearly as more data types contribute positively to the sum, the sum increases monotonically. However, if there are five strong positive data contributions of elevated heat from five different data types for example, then adding a sixth positive contribution does not provide much new information. This aspect is taken into account with the logistic link, or *expit* function, $Pr = \exp\mathrm{it}(\Sigma) = e^{\Sigma}/[1 + e^{\Sigma}] = [1 + e^{-\Sigma}]^{-1}$ (Eq. (1)), which spans 0–1 as does a true probability. In another location the sum $\sum$ could be large and negative, in which case the probability of heat will be small. In yet another location where there are no data, the data votes will be zero, but the probability will not be; it will equal the prior probability $Pr_0 = \mathrm{expit}(w_0) = [1 + e^{-w_0}]^{-1}$. The probabilities of elevated permeability and fluid are computed in the same way.

Using the marginal probabilities of all three resource qualities (Pr_H, Pr_P, Pr_F), we approximate the probability of a viable resource Pr_R by the product of the marginals,

$$\mathrm{Pr}_R(\mathbf{x}) = \mathrm{Pr}_H(\mathbf{x})\mathrm{Pr}_P(\mathbf{x})\mathrm{Pr}_F(\mathbf{x}). \quad (2)$$

This equation is the second building block of our method; like Eq. (1), it is based on a conditional independence assumption that has a long record of surprising robustness in Bayesian learning (e.g., Domingos and Pazzani, 1997; Porwal et al., 2006). We refer to Eq. (2) as the "veto equation" because if any one quality has a low probability, so will the probability of a viable resource. The output probabilities are evaluated at each 200 m × 200 m cell of the model grid, the centers of which define $\mathbf{x}$. The calculations were performed primarily and displayed entirely using Generic Mapping Tools (GMT) (Wessel et al., 2013). Some of the calculations, prior to visualization, were done using Matlab® (www.mathworks.com).

2.2. Specifics: expert elicitation and defining weights (w_i)

The voter Eq. (1) requires converting the starting data value D_i to its processed form z_i, and relating the importance of the data, quantified by its weight w_i, to the probability of a given resource quality. In this knowledge-driven, reconnaissance application, we use *expert elicitation* (e.g., O'Hagan et al., 2006; O'Leary et al., 2009). As such, the prospecting algorithm incorporates the expertise of our research team, and is thus able to "think" like an expert with years of experience. To understand how we do this, consider first the baseline probability value Pr_0 for a given resource quality (*H*, *P*, or *F*). We ask the expert for the probability of that quality at an unknown location. The expert knows only that the location is in Hawaii, and is free to solve the question in any way he or she wishes. We then set the expert's estimated probability Pr_0 equal to $\mathrm{expit}(w_0)$ and solve for w_0, using the inverse function,

$$w_0 = \mathrm{logit}(Pr_0) \equiv \ln\left(Pr_0/(1 - Pr_0)\right). \quad (3)$$

To incorporate input from multiple experts, we weight by years of experience and take the weighted average of their respective values of w_0.

Now consider how to elicit the effects of the first data type D_1 (e.g., gravity) on the probability of a resource quality, for example heat Pr_H. We seek to define z_1 and w_1 so that with only that data type appearing in the sum of the voter Eq. (1), the resulting values of Pr_H at one or two values of D_1 are consistent with the expert's intuition. (I) First, we give each expert in our team a particularly promising data value in either its starting D_1^+ or processed z_1^+ form (whichever is more intuitive to the expert), and ask them to estimate the corresponding probability Pr_H^+. (II) Second, we then ask the expert to estimate the value, D_1^- for which the data has no effect on probability. Question (I) is used to establish the *location* property—i.e., what Pr_H is at a given D_1 (or z_1) —for the dependence of Pr_H on D_1 alone. With the answer to question (I), question

Table 1
Summary of data types used in this study and evidence they provide as explained by Lautze et al. (2016a).

Data Type	Evidence Pertaining to Elevated Heat
Gravity	High values indicate dense intrusive source rock
Geologic mapping of rift zones and calderas	Probable location of intrusive source rocks
Geologic mappings of volcanic vents	Possible locations of intrusive source rock
Groundwater Cl/Mg	High values occur in geothermally altered seawater due to the preservation of dissolved Cl but loss of Mg to precipitated minerals
Groundwater SiO_2	High values can indicate greater solubility of SiO_2 in geothermal water
Groundwater temperature	Values elevated compared to local ambient temperatures indicate mixing with geothermal fluids
Electrical resistivity	Low values can indicate hot water, rock, or magma
Data Type	**Evidence Pertaining to Elevated Permeability**
Gravity	High values indicate dense intrusions above which faulting and rifting occur
Geologic mapping of rift zones and faults	Where permeability is enhanced by fracturing.
GPS measurements of ground displacement	Areas of dilation indicate where permeability is being enhanced by fracturing
Seismicity	High seismicity occurs where the crust is already weak and permeable, or where fracture permeability is being enhanced
Data Type	**Evidence Pertaining to Adequate Fluid**
Water table elevation	High values increase the probability of high fluid pressure and thus hotter water near the source rock
Ground water recharge	High values indicate enhanced fluid content and pressure
Resistivity	Low values can indicate high fluid content

(II) is used to establish the *scale* property of the function—i.e., how quickly $\Pr_H$ varies with D_1. In all cases, we require question (I) to be answered. For some data types, however, question (II) cannot be confidently answered, in which case, the scale parameter comes from the data themselves as the variation within the population of measurements obtained. With both questions addressed, D_1^+ is transformed and scaled to produce z_1^+, Pr_H^+ is set equal to $\text{expit}(w_0 + w_1 z_1^+)$, and then we solve for w_1 using the logit function defined in Eq. (3). We repeat this process for data type 2, then data type 3, and so forth, continuing in this way until we obtain all the necessary data weights.

2.3. Specifics: data transformation and scaling (converting D_i to z_i)

Transformation and scaling are done to facilitate the process of accurately producing a dependence of probability on D_i consistent with the expert knowledge. Transformation ensures that the processed data, z_i is unbounded (theoretically spanning $\pm\infty$) as is needed by the voter Eq. (1); scaling normalizes the values of z_i for the different data types so that they have comparable meaning, even though the starting data may be given in different units and widely different numerical values. To illustrate, we describe the transformation and scaling functions for two example data types.

The first example is how the probability of permeability $\Pr_P$ is influenced by the frequency of earthquakes on Hawaii Island. Seismicity is an indication of fracturing, a promoter of fracture permeability (Tilling et al., 1987; Martel and Langley, 2006; Ingebritsen and Manning, 2010), and is more likely to occur where the crust is already weak and permeable (P. Okubo pers. comm. 2015). Consequently, our experts estimated that the $\Pr_P$ should be high ($Pr_P^+ = 0.8$) where seismicity is *unusually high* (question (I)). However, they could not estimate the rate at which $\Pr_P$ should change with seismicity (question (II)). With seismicity (events per km^2 per yr) within each geographic grid being the starting data value D_2, the transformation is

$$d_2 = \ln(D_2), \quad (4)$$

and scaling is done by standardization,

$$z_2 = \frac{d_2 - \hat{d}_2}{\sigma_2}. \quad (5)$$

Here $\hat{d}_2$ is the median value of the transformed seismicity, and σ_2 is given by the median absolute deviation:

$$\sigma_2 = 1.482 \times \text{median}(|d_2 - \hat{d}_2|), \quad (6)$$

in which the factor 1.482 reproduces the standard deviation if d_2 is normally distributed. Eq. (4) transforms the population of starting measurements, which is bounded on one side by 0, to the domain $(-\infty, +\infty)$ with a more symmetric distribution about the median. The *unusually high* value of seismicity in question (I) was defined by the experts in terms of the standardized value, $z_2^+ = 1.5$ and establishes the *location* property of the dependence of $\Pr_P$ on seismicity. The variability within the transformed data population, σ_2, sets the *scale* property that controls how quickly $\Pr_P$ varies with D_2, again because question (II) could not be answered. Finally, we obtain the weight w_2 as the solution to $Pr_P^+ = 0.8 = \text{expit}(w_0 + w_2 1.5)$, using the logit function, $w_2 = [\text{logit}(0.8) - w_0]/1.5$.

The second example addresses how $\Pr_H$ is influenced by the proximity to a mapped rift zone together with the time since the rift zone was active. With distance to the nearest rift zone being the starting data value denoted as D_3, and the age of the end of the shield volcanic stage of that volcano denoted as t, the transformation function is

$$z_3 = \text{logit}\left\{\left(\frac{r_0}{d_3 + r_0}\right)^2 \left(\frac{t_0}{\tau + t_0}\right)\right\}, \quad (7)$$

where $d_3 = \max(D_3, r_{\min})$ and $\tau = \max(t, t_{\min})$.

The argument of the logit function in Eq. (7) has the range (0, 1) if the lower limits, $r_{\min}$ and $t_{\min}$, are both zero, in which case the logit maps its argument into $(-\infty, +\infty)$. The singularities that occur when $D_3 = 0$ km and $t = 0$ Myr are avoided by setting non-zero lower limits on d_3 and τ. Within the argument, the inverse square relation with d_3 represents a reduction in the frequency of intrusive source rock, and hence $\Pr_H$, with distance from a rift zone. The mathematical form of this decay follows that of the decay of stress perturbation away from a two-dimensional (2-D) (infinitely long in one direc-

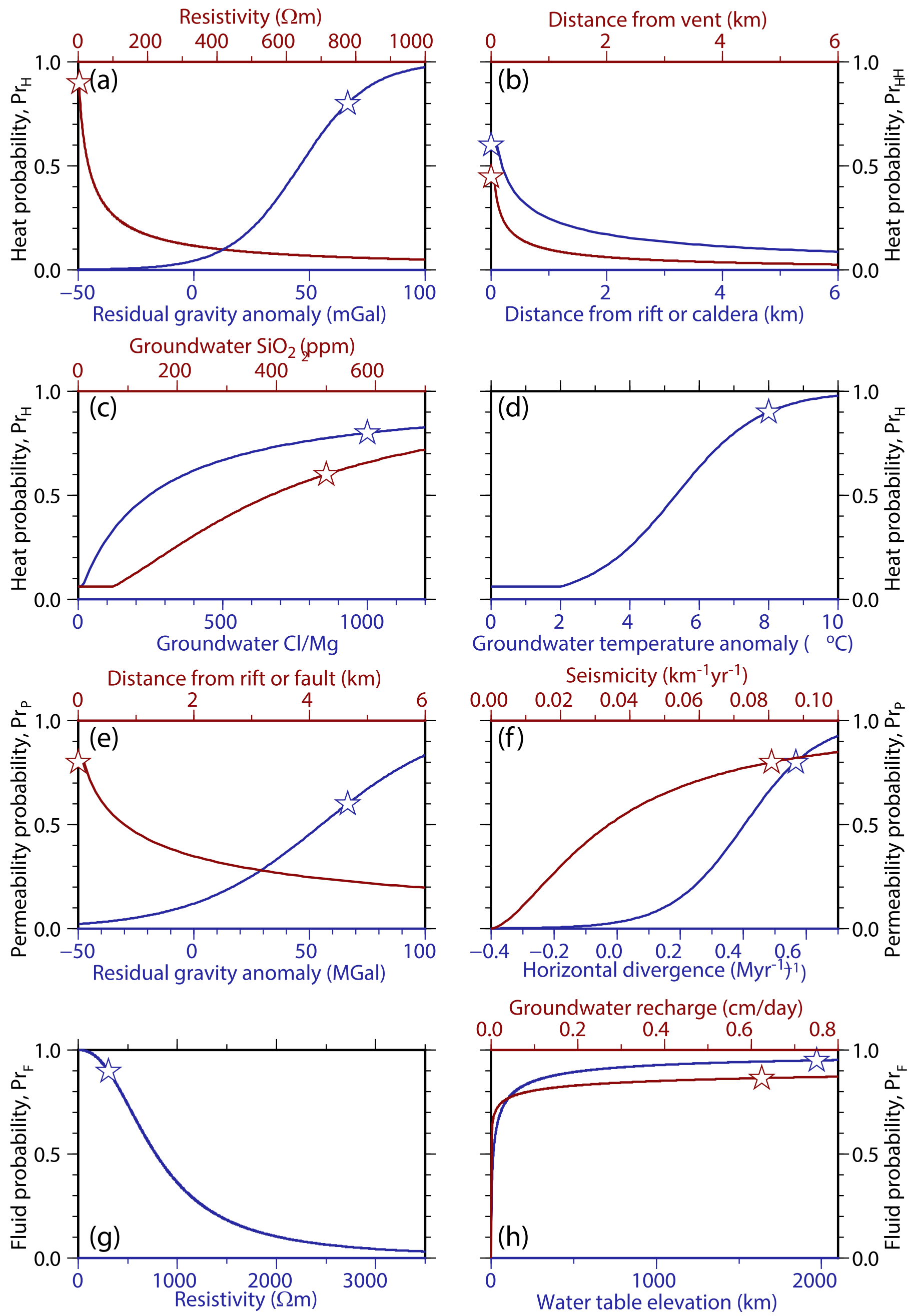

Fig. 1. Marginal probability functions of elevated heat (a)–(c), permeability (d)–(e), and fluid (f)–(g) due solely to the individual data types labeled on the horizontal axes. Two data types shown in a panel are distinguished by colors of the curves and axis labels. Stars indicate promising data values D_i^+ at which the probabilities Pr^+ were estimated by experts.

tion) crack in a homogeneous elastic medium (Pollard and Segall, 1987)—the crack representing the intrusive complex beneath the rift zone. The inverse time relation comes from the Green's function for2-D diffusion (Sommerfeld, 1964). The minima r_{min} and t_{min} establish the *location* properties by specifying the distance-age combination at which $Pr_H = Pr_H^+$, whereas r_0 and t_0 establish the *scale* properties that control how quickly Pr_H changes with distance and age, respectively.

For all data types, the transformation and scale functions, as well as the values of the associated parameters and weights are given in Table 2 and justified below in Section 3. The resulting dependencies of probability on each data type individually are shown in Fig. 1.

2.4. Confidence

A simple measurement of the confidence in the marginal probability estimate for each resource quality (*H*, *P*, *F*) uses a modified form of the voter equation.

$$C(\mathbf{x}) = \left[1 + \exp\left(-w_0 - \sum_{i=1}^{m} w_i z_i^+ q_i(\mathbf{x})\right)\right]^{-1} \tag{8}$$

Here the quality factor ($0 < q_i \leq 1$) is assigned by the expert to data type *i*; again z_i^+ is the transformed and scaled form of the promising data value D_i^+ used during expert elicitation, and the product $w_i z_i^+$ is always positive. The sum in (8) is over only the *m* data types that are present in the model grid cell centered on $\mathbf{x}$. A modified veto

Table 2
Quantities and equations for data processing and conversion to probability.

Heat, $Pr_0 = 0.06$, $w_0 = -2.75$							
Starting data, D	Transformation and scaling	Median & σ	Adjustments	Promising values, D_i^+; z_i^+	Pr_H^+	w_i	q_i
Residual gravity anomaly (mGal)	$d = D\frac{t_0}{(t+t_0)}$, $t_0 = 0.1$ Myr[a]; then standardized (Eq. (5)) to give z	4.73; 9.63	none	66 mGal (=1.5 σ at $t = 0$ Myr); 6.40 including all t	0.8	0.65	0.75
Distance from nearest caldera, rift zone, or rift-zone vent (km)	$z = \text{logit}\left\{\left(\frac{r_0}{d+r_0}\right)^2\left(\frac{t_0}{\tau+t_0}\right)\right\}$ $d = \max(D, 1.5\text{ km}), \tau = \max\left(t, 10^{-6}\text{ Myr}\right)$, see Eq. (7); $r_0 = 25$ km[b]; $t_0 = 0.7$[a]	n/a	none	0 km; 4.8	0.6	0.65	0.75
Distance from nearest non-shield-stage volcanic vent (km)	$z = \text{logit}\left\{\left(\frac{r_0}{D+r_0}\right)^2\left(\frac{t_0}{t+t_0}\right)^{3/2}\right\}$ Lower limit on D is 0.05 km; lower limit on t is 10^{-6} Myr. $r_0 = 5$ km[c]; $t_0 = 0.8$ Myr[d]	n/a	none	0 km; 3.9	0.45	0.65	0.75
Groundwater temperature (°C)	$d = D - (T_s - 3 + 5.29\,Z)$; T_s is ambient local surface temperature, Z is depth. d is then standardized to give z'	−0.100; 2.08	$z = \max(z', 1) - 1$ and projected up flow paths	8 °C; 3.9	0.9	1.7	0.25
Cl/Mg ratio	$z' = \ln\left(\frac{D}{D^-}\right)$ $D^- = 15$	n/a	$z = \begin{cases} 0, & z' < 1 \\ z', & z' \geq 1 \end{cases}$ projected up flow paths	1000; 4.2	0.8	0.99	0.25
SiO_2 (ppm)	$d = \ln(D)$; then standardized (Eq. (5)) within each watershed to give z'	3.85; 0.400	$z = \max(z', 1) - 1$ and projected up flow paths	500 ppm; 5.9	0.6	0.64	0.25
Resistivity from MT (Ωm)	$d = \ln(D/250)$	n/a	none	3 Ωm; −4.42	0.9	−1.12	0.75

Permeability, $Pr_0 = 0.14$, $w_0 = -1.82$							
Starting data, D	Transformation and scaling	Median & σ	Adjustments	Promising values, D_i^+; z_i^+	Pr_P^+	w_i	q_i
Residual gravity anomaly (mGal)	same as for heat	4.73; 9.63	none	66 mGal (1.5 σ for $t = 0$ Myr); 6.4	0.6	0.35	0.75
Distance from nearest caldera, rift zone or fault (km)	same as for heat	n/a	none	0 km; 4.9	0.8	0.66	0.75
Mean ground displacement rates, (Myr^{-1})	$d = (\nabla \cdot \mathbf{v})_h$ then standardized (Eq. (5))	0.19; 0.25	none	$d = 0.57$ Myr^{-1}; 1.5	0.8	2.1	0.5
Seismicity (number of events per km^2 per yr)	$d = \ln(D)$ then standardized (Eq. (5))	−4.52; 1.33	none	0.081 km^{-2}yr^{-1}; 1.5	0.8	2.1	0.25

Fluid, $Pr_0 = 0.78$, $w_0 = 1.27$							
Starting data, D	Transformation and scaling	Median & σ	Adjustments	Promising values, D_i^+; z_i^+	Pr_F^+	w_i	q_i
Groundwater Recharge (cm/day)	$d = \ln(D)$ then standardized (Eq. (5))	−2.96; 1.66	none	1.87 cm/day; 1.5	0.87	0.39	0.75
Water table elevation (m)	$d = \ln(D)$ then standardized (Eq. (5))	4.76; 1.89	none	1970 m; 1.5	0.95	1.1	0.5
Resistivity (Ωm)	$d = \ln(D/450)$	n/a	none	300[g] Ωm; −0.40	0.90	−2.3	0.75

[a] These values of t_0 in the shown functions cause probability to decay with time in proportion to the decay of heat with time at the center of an infinitely long prism having width and height of 5 km. 5 km is the approximate width of the P-wave tomography anomaly beneath Kilauea's SW rift zone (Okubo et al., 1997).
[b] $r_0 = 25$ km leads to a reduction of probability to the prior Pr_0 at a distance of 10 km, or twice the characteristic width of Kilauea's rift zone.
[c] $r_0 = 5$ km leads to a reduction of probability to the prior, Pr_0 at a distance of 2 km away from the center of a post-shield or rejuvenated volcanic vent.
[d] This value of t_0 causes probability to decay with time approximately in proportion to the decay of heat with time at the center of a cubed shaped intrusion 1 km on a side.

equation determines the confidence of the estimated probability of a geothermal resource,

$$C_R(\boldsymbol{x}) = C_H(\boldsymbol{x})C_P(\boldsymbol{x})C_F(\boldsymbol{x}). \tag{9}$$

Thus, each probability computed by our method has an associated confidence. For example, if a given location has many types of high quality data, and none of those data types suggest a resource, the probability of a resource at that location will be very small, but our confidence in that probability will be high. A low confidence equates to a lack of high quality data, a situation in which additional data are needed to adequately assess resource probability. Together with probability, confidence can be used to prioritize the locations and nature of future exploration efforts.

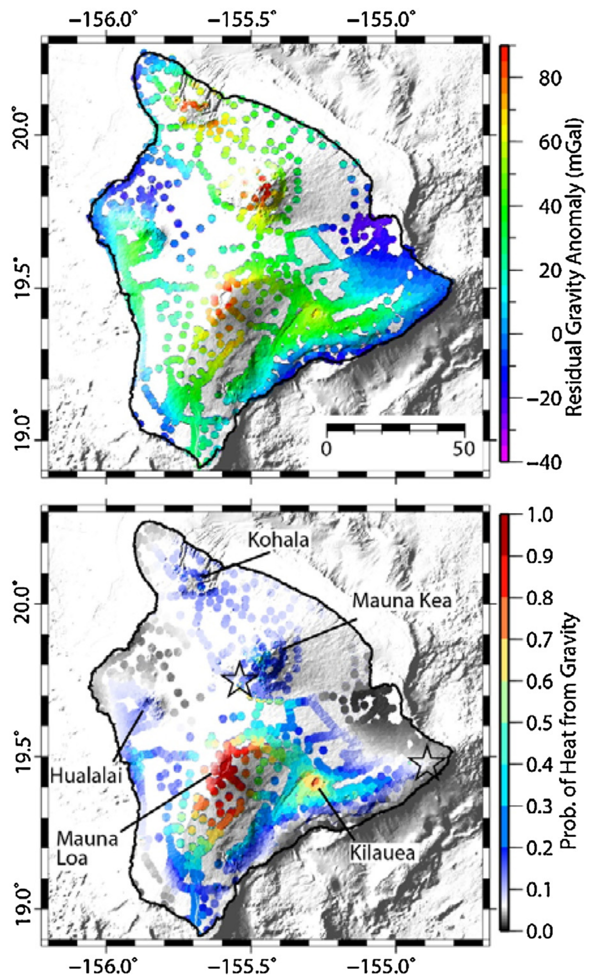

Fig. 2. (a) Residual gravity anomaly of Hawaii Island (outlined in black) is shown as colored circular patches, 3 km in diameter around each measurement. Topography is shown by illumination from the NW. White indicates no data. (b) The effects of gravity alone on the probability of heat Pr_H. Within the island boundary, white indicates the prior probability, $Pr_0 = 0.06$; gray shading darkens as values decrease below Pr_0. Shield volcanoes are labeled; stars indicate locations of the Saddle drill site (north) and the Puna Geothermal Ventures (PGV) geothermal power plant (south).

3. Specific data types and their impact on marginal probabilities ($\mathbf{Pr}_H$, $\mathbf{Pr}_P$, $\mathbf{Pr}_F$)

3.1. Gravity and MT data

Gravity is sensitive to crustal density and thus is used as an indicator of dense intrusions. These intrusions are the geothermal heat sources and they can enhance permeability by causing faulting and fissuring during or shortly after emplacement. The starting data D is the residual gravity anomaly of Flinders et al. (2013) (Fig. 2). It is the complete Bouguer anomaly minus the attraction of the crust-mantle interface assuming it bows downward below the islands with a flexed elastic lithospheric plate. These data were interpolated onto the model grid as circular patches 3 km in diameter, centered on each measurement using GMT's *nearneighbor* routine.

The transformation of the starting data involves accounting for the effects of cooling of intrusive rocks (see Table 2),

$$d = D\frac{t_0}{(t + t_0)}. \tag{10}$$

Here t is the age of the youngest date of the volcanic stage associated with the surface lava at each point across the state (shield stage dates from Bianco et al. (2005) and references therein), and the inverse age relation is the same as in Eq. (7). A lower limit of $t_{min} = 10^{-6}$ Myr (see Eq. (7)) and the time scale $t_0 = 0.7$ Myr leads to a decrease in probability with time in proportion to the decay of heat with time at the center of an infinitely long (2-D) prism having a thermal diffusivity of 10^{-6} m^2/s (Turcotte and Schubert, 2002) and square cross-section of dimension 5 km. The prism is a crude representation of the intrusive complex beneath a volcanic rift zone with a width comparable to that imaged seimically beneath Kilauea's rift zone (Okubo et al., 1997). The same age decay was applied when modeling the effects of gravity on the probabilities of elevated heat as well as permeability. Permeability is expected to decay with age as pore-space is reduced due to erosion, mass-wasting, and mineralization. The transformed data d, were then standardized (Eq. (5)).

The "favorable" condition for residual gravity anomaly is $D^+ = 66$ mGal (=1.5σ) at zero-age; the corresponding probabilities of heat and permeability were estimated to be $Pr_H^+ = 0.8$ and $Pr_P^+ = 0.6$, respectively. The resulting weights (Table 2) lead to the probability functions shown in Fig. 1a and e. Pertaining to heat, a map view of Hawaii Island, for example, shows that the active volcanoes, Mauna Loa and Kilauea, in the south have high gravity anomalies and high probabilities (Fig. 2). The older volcanoes ($t = 0.25$ Myr for Mauna Kea; $t = 0.3$ Myr for Kohala) have comparably high gravity anomalies but lower probabilities reflecting the age correction.

The electrical resistivity used in this study are the inversion results of a magnetotelluric (MT) survey (Pierce and Thomas, 2009) just south of Mauna Kea on Hawaii Island. Near this location is the Humu'ula Saddle groundwater exploration well, where a geothermal system was discovered (Fig. 3b). The starting data are the mean resistivity values below the surface within 500 m of sea level. These data were normalized by a scaling factor determined from the answers to question (II) for heat and permeability, and then log-transformed and standardized (see Eqs. (4) and (5) and Table 2). The effects on the probability of excess heat and fluid are shown in Fig. 1a and g, respectively, and appear on Hawaii Island as locally high (and a couple of low) values along an arc wrapping around the southern flank of Mauna Kea volcano (Fig. 3b and h).

3.2. Proximity to calderas, rift zones, volcanic vents, and faults

Proximity to the shield-stage features—caldera, rift zone, and rift-zone volcanic vent— pertains to the probability of elevated heat Pr_H. Proximity to rift zones and faults pertains to the probability of permeability Pr_P. The starting data D is the distance of the map cell from the closest geologic feature. The age t is the time since the end of the shield stage associated with that feature. Data transformation and scaling are described by Eq. (7) and Table 2. For zero-age calderas and rift zones, $r_{min} = 0.1$ km and $r_0 = 25$ km lead to a reduction in probability from their promising values ($Pr_H^+ = 0.6$; $Pr_P^+ = 0.8$) directly on the feature ($D = 0$ km) to the prior values at a distance of $D \approx 10$ km (Fig. 1b and e). This distance is about twice the width of the P-wave seismic anomaly marking the intrusive zone beneath Kilauea's east rift zone (Okubo et al., 1997). The age parameters $t_{\rm min}$ and t_0 are given in Table 2.

The probability of elevated heat Pr_H is also influenced by the distance to the nearest post-shield and rejuvenated volcanic vents. The distance function (7) with $r_{min} = 0.05$ km and $r_0 = 5$ km leads to a decay of Pr_H from the promising value ($Pr_H^+ = 0.45$) on a vent, to the prior Pr_0 at a distance of $D \approx 2$ km (Table 2, Fig. 1b) at zero age. The decay with age of the vent t is quicker than that for a 2-D feature such as a rift zone (Table 2); the $t^{-3/2}$ dependence comes from the Green's function for time-dependent heat diffusion in three-dimensions (3-D) (Sommerfeld, 1964). Parameters $t_{min} = 10^{-6}$ Myr and $t_0 = 0.8$ Myr lead to a rate of decay right on a vent ($D = 0$) that is approximately proportional to the decay of heat at the center of a cube-shaped intrusive body 1 km on a side.

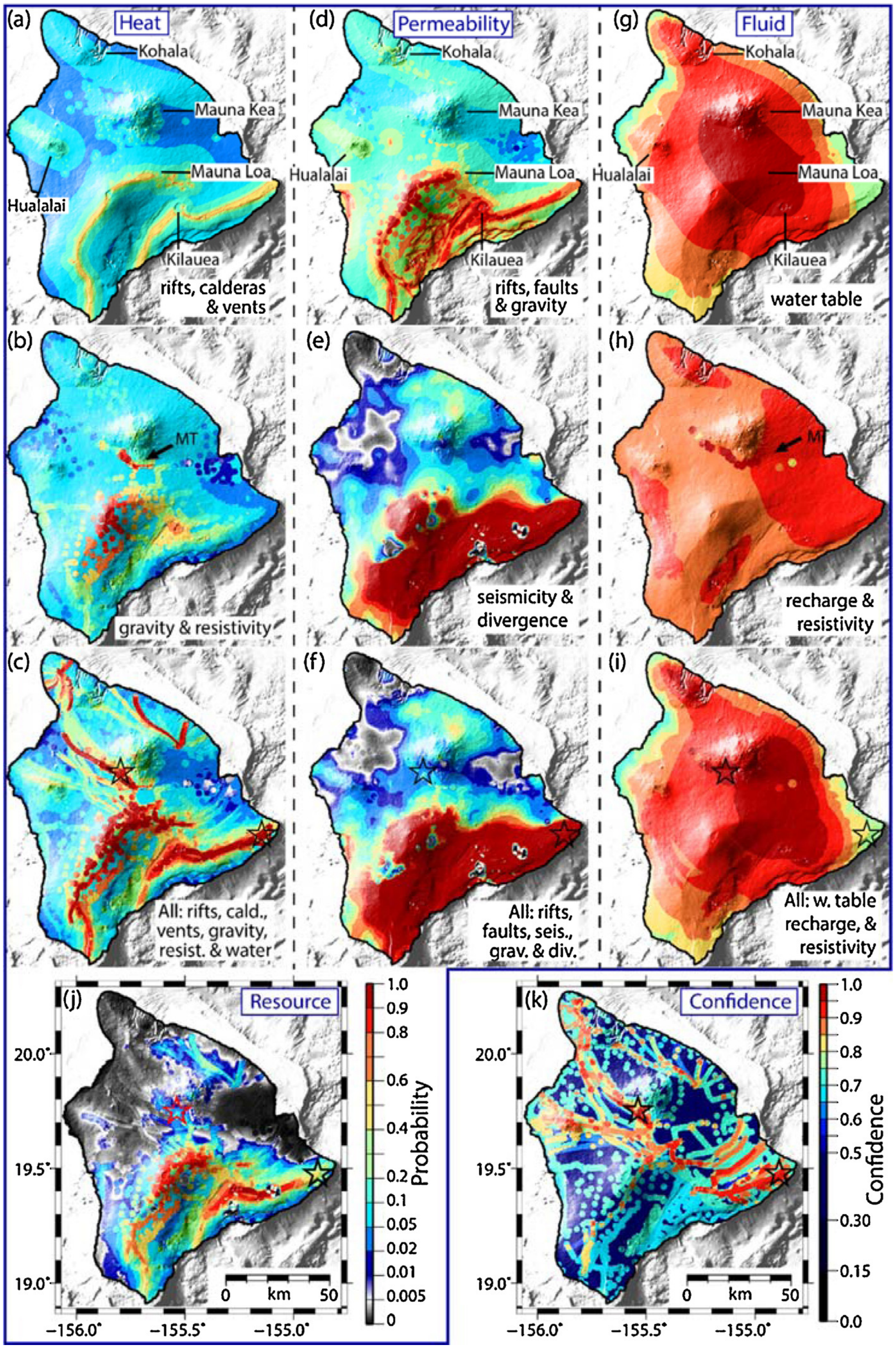

Fig. 3. Predicted marginal probabilities of elevated (a–c) heat, (d–f) permeability, and (g–i) fluid when the effects of only the listed data types are included in the voter equation (1). The "MT" survey is marked in (b) and (h). The product of (c), (f), and (i) gives (j) the probability of a resource (Eq. (2)). Probabilities are colored according to the same non-linear scale; white indicates probabilities equal to the product of the prior probabilities of heat, permeability, and fluid; gray-to-black indicates probabilities less than the product of the priors. (k) Confidence in the resource probabilities. Stars indicate locations of the Saddle drill site (north) and PGV power plant (south) as in Fig. 2.

The final effect on $\Pr_H$ is either that due to proximity to a shield stage feature *or* that due to a post-shield/rejuvenated stage vent, whichever feature is closer to the cell location $\mathbf{x}$. On Hawaii Island, the most positive contributions to $\Pr_H$ (Fig. 3(a)) as well as $\Pr_p$ (Fig. 3(d)) occur on the active shield-stage volcanoes in the south, and less positively on the older volcanoes.

3.3. Well water data

Groundwater temperature is a direct indicator of elevated crustal heat at present-day. The transformation step involved first subtracting the mean local surface temperatures T_s from the measured water temperatures. We then found the best-fitting line to all excess temperatures versus depth Z, and subtracted that line from each measurement (Table 2). The resulting temperature anomalies d were then standardized.

We then made two adjustments. The first is a thresholding step in which we considered only standardized values exceeding unity; thus

$$z = \max(z\prime, 1) - 1, \qquad (11)$$

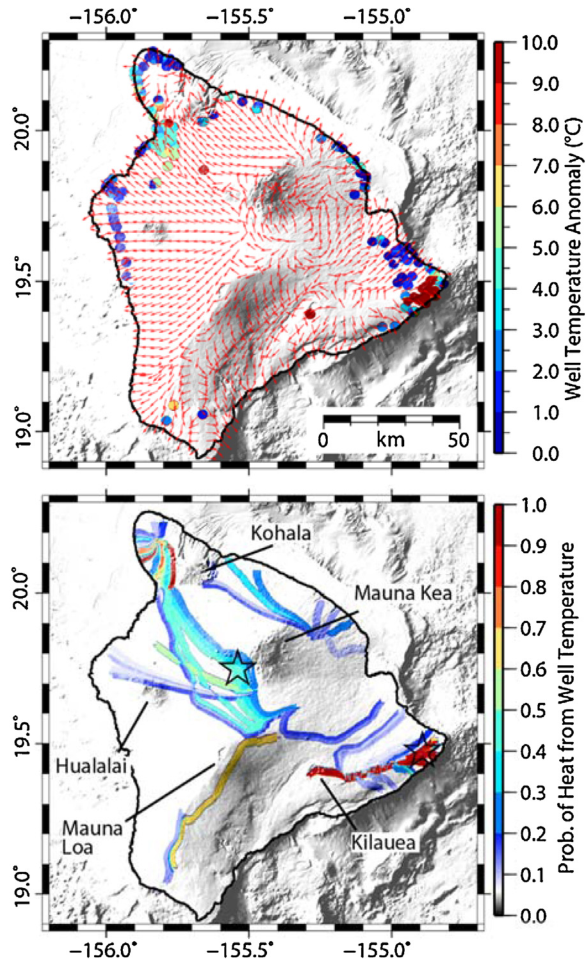

Fig. 4. (a) Water well temperature in excess of surface temperature and corrected for depth (Table 2) are shown as colored patches at well locations. Red arrows show model groundwater flow directions. (b) Probability of heat due to water temperature anomaly after projecting the effects back up flow paths. Stars are as in Fig. 3. (For interpretation of the references to colour in this figure legend, the reader is referred to the web version of this article.)

in which the original standardized value is denoted here by z'. Preventing low values from impacting probability accounts for heat loss due to mixing and diffusion: we avoid reducing probability in the situation in which geothermal water is present but has been cooled. A threshold of 1 (i.e., excess temperature of 1σ) accounts for the typical fluctuations at each well, for example, related to seasonal variability. The resulting probability of excess heat decreases from $\mathrm{Pr}_H = 0.9$ at $D^+ = 8\,°\mathrm{C}$ to the prior probability at the corresponding threshold temperature of 2.08 °C (Fig. 1d).

The final adjustment accounts for the fact that Hawaii's groundwater can flow many tens of km, and so the well location where the temperature was measured is a poor estimator of the actual location of the geothermal source. We therefore used groundwater flow models produced by the Hawaii State Department of Health (Rotzoll and El-Kadi, 2007; Whittier and El-Kadi, 2014) to estimate the flow path to the well (Fig. 4(a)). All grid locations on that path were then assigned the threshold-adjusted value of the standardized data z. These projected values were then used in the voter Eq. (1) to estimate the probability of elevated heat at all possible locations of the heat source. On Hawaii Island, the results show maximal values of Pr_H along Kilauea's East Rift Zone, near the one geothermal power plant in Hawaii, which is run by Puna Geothermal Ventures (PGV) (Fig. 4(b)).

Cl/Mg and SiO_2 are the two groundwater chemical indicators of geothermal heat. The starting data D are the measured Cl/Mg ratio and SiO_2 in ppm (Table 2). For Cl/Mg (Fig. 1c), standardization was not needed because the experts estimated (question (II)) that its effects on Pr_H should be negligible at a ratio of $D^- = 15$, the approximate upper-bound of the range of Hawaii's normal groundwater (Cox and Thomas, 1979). The transformed and scaled data is $z' = \ln(D/D^-)$, but only ratios of $d > 15$ were considered to avoid any influence by normal groundwater. For SiO_2, the question (II) of scaling could not be answered so standardization was needed. In this case, standardization was done using only measurements within the local watershed to account for local processes other than geothermal activity such as agricultural practices that can influence groundwater silica concentrations. Thresholding was done for SiO_2 as well so that only standardized values in excess of 1.0 indicate positive evidence for geothermal heat, again to account for the effects of mixing. For both Cl/Mg and SiO_2, the threshold-corrected z values were projected up groundwater flow trajectories as was done for water temperature.

On Hawaii Island, the effect of groundwater chemistry and water temperature on Pr_H are discernable by comparing Fig. 3(c) to (a) and (b). Combined with the effects of the other data types, the water data contribute to maximal probabilities for excess heat along Mauna Loa's, Kilauea's, and Kohala's rift zones, west and south of Mauna Kea, and around Kohala's summit.

3.4. Ground deformation and seismicity

Ground deformation is associated with the creation of crustal permeability and is estimated based on the relative motion recorded by the permanent GPS network on Hawaii Island (Brooks et al., 2006). Most of the stations are on Kilauea and Mauna Loa, but there are a handful of stations around the perimeter of the island to the north. The GPS network is restricted to Hawaii Island, so that was the only island for which GPS data were used. Mean velocities were computed over the life-time of each GPS station, and interpolated onto a regular grid using 2-D splines(Wessel et al., 2013). The east and north component of the gradients of the east and north velocities ($\partial v_x/\partial x$ and $\partial v_y/\partial y$) were then computed at each grid point on Hawaii Island. The sum of the two is the horizontal part of the divergence $(\nabla \cdot \mathbf{v})_h$, which is >0 for expansion and <0 for contraction. These transformed data $d = (\nabla \cdot \mathbf{v})_h$where then standardized. Using only divergence, the probability of permeability decreases from the favorable value of $Pr_P^+ = 0.8$ at $(\nabla \cdot \mathbf{v})_h = +0.57\,\mathrm{Myr}^{-1}$ $(z^+ = 1.5)$ to the prior probability of elevated permeability, $\mathrm{Pr}_0 = 0.14$ at $(\nabla \cdot \mathbf{v})_h = +0.19\,\mathrm{Myr}^{-1}$ $(z = 0)$ (Fig. 1f, Table 2).

Seismicity is another indicator of permeability. Our treatment of seismicity was summarized above in Section 2.3 and is detailed here. Specifically, we used the earthquakes identified and relocated by Matoza et al. (2013) on and around Hawaii Island for the period of 1992–2009. For the other islands, seismicity was not studied and is not used here. As we are interested in the shallow crust, the data are restricted to the ~40,000 events at depths ≤5 km. Seismicity, S, is the starting data D. It is the number of earthquakes per unit of geographic area per year estimated using the distance-weighted average,

$$S(\mathbf{x}) = \frac{\sum_i f(|\mathbf{x} - \mathbf{x}_i|)}{\Delta t \int_0^{R_s} \int_0^{2\pi} f(r) r d\theta dr} \tag{12}$$

Here $r = |\mathbf{x} - \mathbf{x}_i|$ is the radial distance between the cell location $\mathbf{x}$ and seismic event i within the averaging window of radius $R_s = 5\,\mathrm{km}$;

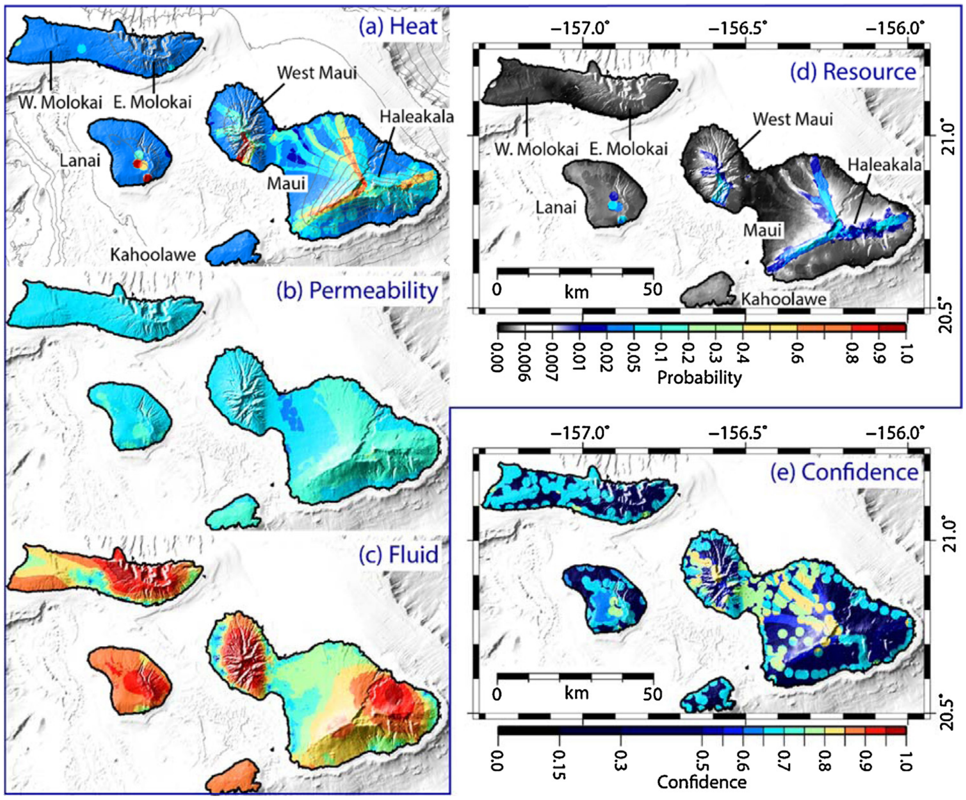

Fig. 5. Marginal probabilities of elevated (a) heat, (b) permeability, and (c) fluid for the Maui Nui island group. Also shown are the (d) final resource probability and (e) confidence in those probabilities. Color scheme is the same as that for Hawaii Island in Fig. 3.

θ is azimuth and $\Delta t = 17.25$ yrs is the time span of the earthquake record. The distance weighting function $f(|\mathbf{x}-\mathbf{x}_i|) = f(r)$ is a cosine taper that decreases from 1 to 0 as r increases from 1 to R_s and vanishes for $R > R_s$. Again, transformation involved taking the natural log of S and scaling was done by standardization. The resulting dependence of Pr_P on seismicity is shown in Fig. 1f.

On Hawaii Island, the combined effects of ground deformation and seismicity are to produce maximal probabilities ($\mathrm{Pr}_P \sim 0.9$) in the actively deforming areas of Mauna Loa and Kilauea volcanoes (Fig. 3e). They also reduce probabilities below Pr_0 in areas of little activity to the south and north of Kohala volcano.

3.5. Water table elevation and groundwater recharge

The height of the water table above sea level is important in evaluating fluid content because the higher the water table, the greater the water pressure is likely to be in the heat reservoir, and higher pressure increases the boiling point so that water is hotter at a given drilling depth. The importance of water table elevation is based on our assumption that for Hawaii, hydrostatic pressure plays a greater role in reservoir temperature and fluid circulation than do confining layers (e.g. a clay cap) in the stratigraphic section (Lautze et al., 2016a). Water table elevations measured at individual water wells were interpolated on to the model grid of the state using 2-D splines (Wessel et al., 2013). We then took the natural log of these interpolated elevations and standardized relative to the well (not the interpolated) data. Considering only water table elevation, the probability of elevated fluid content decreases from $\mathrm{Pr}_F^+ = 0.95$ at $D^+ = 1971$ m (1.5σ) to $\mathrm{Pr}_F = \mathrm{Pr}_0 = 0.78$ at an elevation of $\sim$120 m (Fig. 1h, Table 2).

The rate of groundwater recharge also influences fluid availability and fluid pressure on the reservoir rock. Recharge models are based on rain gauge data as well as estimates of evapotranspiration and surface water transport; they were produced by the U.S. Geological Survey for the islands of Oahu (Engott et al., 2015) and Maui (Johnson et al., 2014) and from the Hawaii Dept. of Health for the other islands (Whittier, R. pers. comm. 2015). Data processing involved log transformation and standardization (Table 2). Due only to recharge, the probability of elevated fluid content decreases from $\mathrm{Pr}_F^+ = 0.87$ at $D^+ = 0.62$ cm/day ($1.5\,\sigma$) to $\mathrm{Pr}_F = \mathrm{Pr}_0 = 0.78$ at a rate of 0.05 cm/day (Fig. 1h, Table 2).

On Hawaii Island, the water table is highest in the elevated topography between Mauna Loa and Mauna Kea, and recharge is highest on the eastern (windward) slopes of the island. The combined effects on the probability of fluid show high values in the central-eastern part of the island (Fig. 3i).

4. Results: probability of elevated heat, permeability, fluid, and probability of a resource

4.1. Hawaii Island

The marginal probabilities of elevated heat, permeability, and fluid for Hawaii Island are shown in Fig. 3(c), (f), and (i). We emphasize here that the following probability results should be interpreted in terms of their relative, not absolute, values. The probability of elevated heat is greatest at the summits and along the rift zones of the active Mauna Loa and Kilauea volcanoes. Relatively high values are also predicted on the west and southwest flank of Mauna Kea. This prediction is consistent with the findings of the Saddle groundwater drill site of hot (140 °C) water at a depth of 1700 m and a geothermal gradient of $\sim$165 °C/km in the bottom 700 m of the hole. Relatively high values of Pr_H are also present over Kohala's summit and southeast rift zone (i.e., northeast of Mauna Kea). Pr_H is lowest to the east and west of Mauna Kea, in areas far from any mapped rift zones or calderas. The probability of elevated

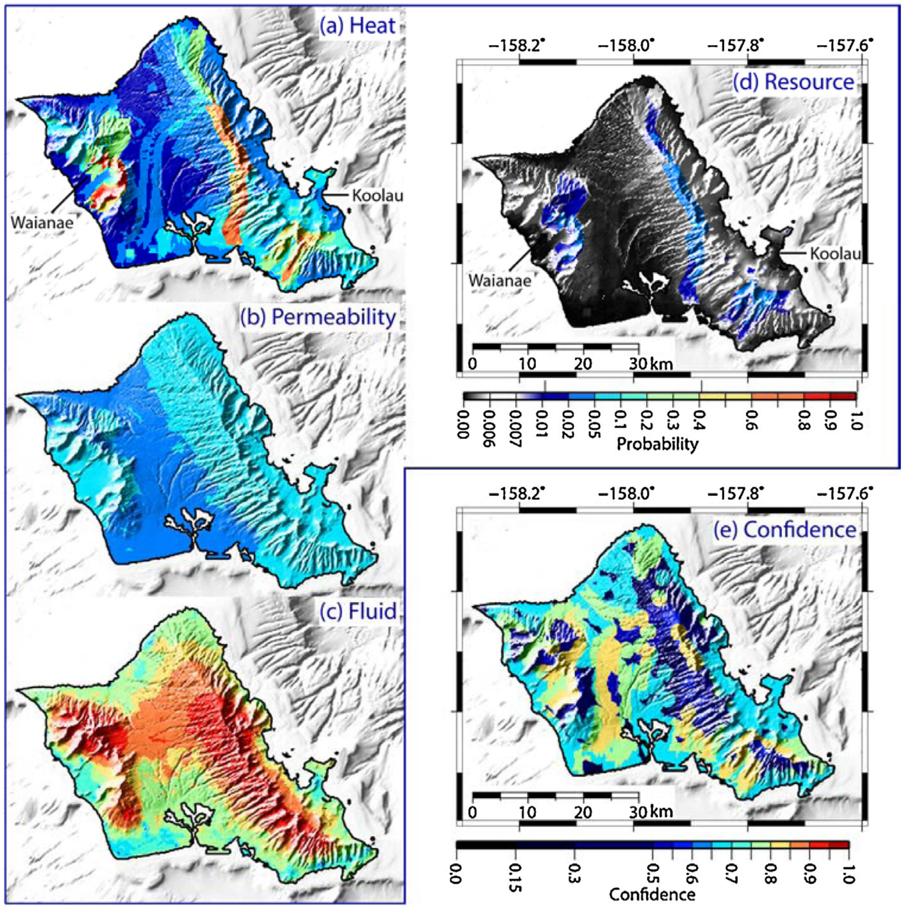

Fig. 6. Results for Oahu are shown just as in Fig. 5. Labels mark the approximate centers of the two shield volcanoes (Sinton et al., 2014).

permeability Pr_P is highest over the whole south and southeast side of the island, largely due to youth as well as the active seismicity and deformation of Mauna Loa and Kilauea. Pr_P is lowest east and west of Mauna Kea and on north Kohala. Finally, the probability of elevated fluid is highest in the central and eastern part of the island and lowest along coasts in the northwest, south, and far east.

The probability of a viable geothermal resource Pr_R is the product of the three marginal probabilities as stated by the veto Eq. (2) (Fig. 3(j)). Near the PGV geothermal plant, resource probability is predicted to be relatively moderate (∼0.4). Confidence (Fig. 3(k)) in this estimate is relatively high (>0.9), owing to the numerous data types in the area, including the overlapping groundwater flow paths associated with well-water indications of elevated heat. The probability of a quality resource is higher further up Kilauea's rift zone and over large areas of Mauna Loa volcano, the highest values being as much as twice that near PGV. Confidence is also relatively high over Kilauea's east rift zone and moderate-to-high (0.5–0.8) on much of Mauna Loa's southwest rift zone. Near the Saddle drill site, Pr_R is low-to-moderate (0.05–0.2), being 10–50% of that near PGV, and confidence is high, especially due to the agreement of the MT survey line as well as the projected water temperature and chemical anomalies. Moderate probabilities, comparable to but less than those at PGV, as well as relatively moderate confidence levels (0.7–0.9) also occur on Mauna Kea's northeast flank and over the summit of Hualalai. Pr_R is minimal with moderate-to-high confidence on Kohala volcano and west of Mauna Kea. Pr_R is minimal with relatively low (<0.5) confidence east of Mauna Kea.

4.2. Maui, Lanai, Kahoolawe, and Molokai

Four islands now make up what was once a much bigger island called Maui Nui. Of these islands, data coverage is most extensive on Maui, as it is the only member of the group for which groundwater flow, recharge, or water table elevation have been evaluated. There are some water well temperatures and chemistry on Lanai and Molokai but not on Kahoolawe. As groundwater flow has not been estimated for Lanai and Molokai the probabilities associated with the groundwater data are estimated only at the locations of the wells on these smaller islands.

The marginal probabilities of elevated heat, permeability, and fluid are shown for these islands in Fig. 5(a)–(c). The mean probability of heat is much lower than that for Hawaii Island due to the greater shield volcano ages (0.6 Myr for Haleakala to 1.6 Myr for East Molokai). On Haleakala, numerous young (0.2–0.6 Myr) post-shield volcanic vents as well as evidence from well-water data lead to moderate-to-high (0.5–0.8) probabilities of elevated heat on the three rift zones. On the south flank of West Maui and central Lanai, water chemistry and temperature lead to elevated values of Pr_H. Probabilities of elevated permeability are also much reduced relative to Hawaii Island due to the greater ages as well as to the lack of seismic or deformation data (and presumably the much lower activity any such data would measure). Of these islands, the younger volcanoes of Kahoolawe and Haleakala show the largest Pr_P values, which are about a factor of two larger than the prior probability of 0.14. The highest probabilities of elevated fluid content are comparable to those on Hawaii Island and occur on the

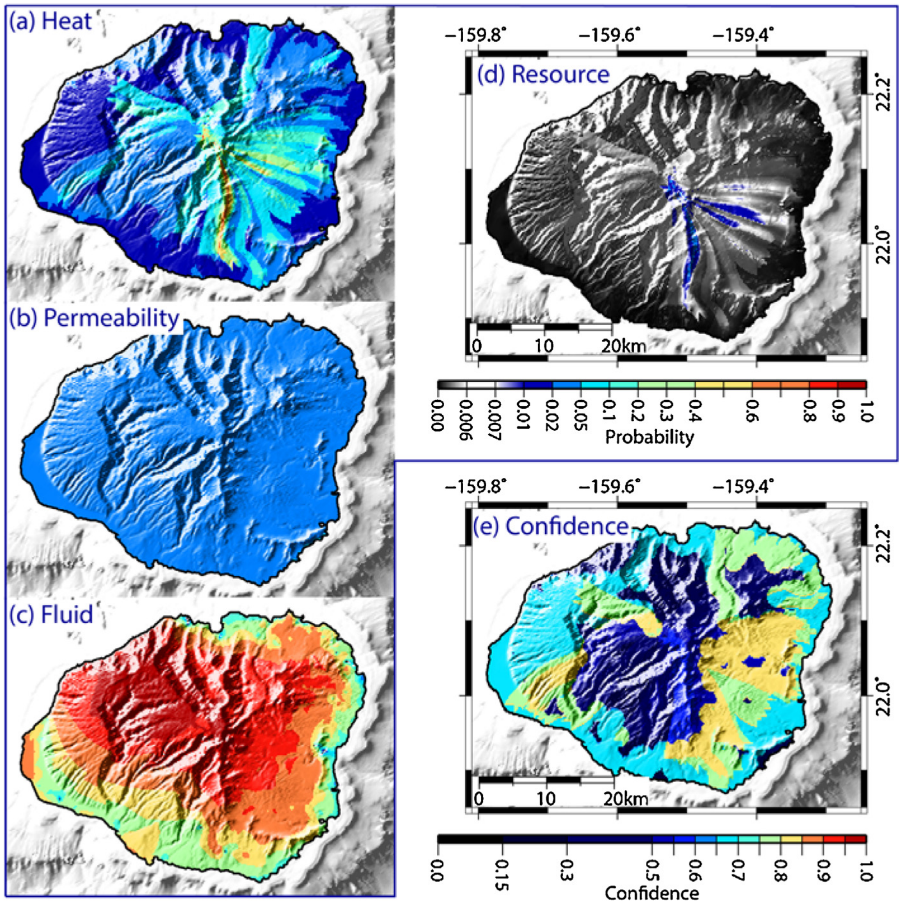

Fig. 7. Results for Kauai are shown just as in Fig. 5.

northeast side of Haleakala, and the summits of West Maui, Lanai, and East Molokai.

The probabilities of a viable resource and confidence in those estimates are shown in Fig. 5(d) and (e). The highest probabilities are 15–20% of that near PGV on Hawaii Island and are comparable to that near the Saddle drill site; these probabilities occur on the southwest, north, and eastern rift zones of Haleakala, on the south flank of West Maui, and in central Lanai. Confidence in those values is relatively moderate (0.6–0.8) on north Halakala and Lanai, and relatively low (<0.5) on West Maui (Fig. 5e). Geothermal resources are least probable between West Maui and Haleakala and on Molokai, especially West Molokai with moderate confidence.

4.3. Oahu

Results for Oahu (Fig. 6) show marginal probabilities of the three resource qualities that span values comparable to those predicted for Maui Nui. Despite the even greater age of Oahu, water temperature and chemistry lead to moderate-to-high probabilities of excess heat in localized areas on the south and southeast of the Koolau shield volcano and the Waianae caldera. The southern edge of the Koolau shield has numerous areas of relatively young (ages < 0.1 Myr) rejuvenated volcanism, which may supply this heat. In contrast, Waianae has no such rejuvenated volcanism. The probability of elevated permeability is low overall, whereas the probability of elevated fluid is high overall, and comparable to that of the other islands.

Resource probabilities on Oahu are predicted to be lower than on Maui and much lower than on Hawaii Island. The highest probabilities with moderate confidence occur on the south flank of the Koolau shield. Here, resource probabilities are about 5% that of the PGV area on Hawaii Island and ~20% that of the Saddle drill site. Slightly lower probabilities at moderate confidence are predicted in the southern part of the Waianae caldera. Probabilities near zero occur in the central part of the island between the two shield volcanoes with moderate confidence.

4.4. Kauai

The results for Kauai—the oldest of the main Hawaiian islands—show the lowest marginal probabilities of elevated heat and permeability across the state (Fig. 7). As a result, the probabilities of a geothermal resource on this island are minimal. Two groundwater flow trajectories extending from the south and east part of the island to the center show Pr_R values just above the prior probability of 0.006, or ~2% of the probability at PGV. The trajectory that starts in Lihue basin on the eastern side of the island has moderate confidence, whereas the southern trajectory has low confidence. Probabilities are near zero elsewhere, especially around the perimeter of the island. Confidence in the probabilities is moderate in all but the most elevated areas of the center part of the island where data coverage is sparse.

5. Discussion and conclusions

We have developed a method of incorporating numerous disparate data types in a quantitative play fairway analysis of natural resources, here applied to geothermal energy in Hawaii. A generalized linear model (i.e., the voter equation) is used to combine evidence provided by the data with expert knowledge, and to calculate probabilities of the key resource qualities of elevated heat, permeability, and fluid. The joint probability of the three qualities, assuming conditional independence (i.e., the veto equation), is then the probability of a successful geothermal prospect. Our method for evaluating the *confidence* in our results is simple, computationally fast, and based on the number of data types associated with each point on the map as well as the experts' estimates of the quality of those data.

Textbooks on statistics often quote Box's aphorism (Box and Draper, 1987), Rule 1: "*All models are wrong but some are useful.*" However, these textbooks often omit Box's equally useful, if harshly stated, Rule 2: "*over-parameterization is often a sign of mediocrity*." We have strived to avoid both over-parameterizing our model as well as over-interpreting its results. With the experts' estimates of probability for a favorable value of a given data type, and in some cases, insight as to how quickly probability should change with the data, only one, or at most two independent parameters define the relationship between the data and probability. The forms of the mathematical relationship are chosen based on physical processes (e.g., decay of stress from a 2-D crack or diffusive cooling) that are assumed to resemble nature. The main results, however, are insensitive to these choices; in developing the method we explored a variety of different mathematical functions and found only minor differences in the final outcomes. We are thus confident that—for better or worse—the predictions of probability honor the knowledge of the experts.

A weakness of the current application is in our mapping of the evidence for excess heat from groundwater temperature and chemistry. First, the results are only as robust as the groundwater flow models, and those have large uncertainties due to the variable spatial distribution of well data used to constrain the models. Second, the method of mapping the effects of the heat indicators back up the groundwater flow trajectories does not account for dispersion. An improvement would be to incorporate dispersion so that the associated trajectory of probability widens with distance up the flow path. Addressing these issues and collecting new groundwater data should be of high priority given that groundwater indicators provides one the most direct ways to detect present-day heat.

Our final results indicate that geothermal resources are most probable and have highest confidence on the active volcanoes of Hawaii island, with some areas showing even greater probability than predicted near Hawaii's PGV geothermal plant on the lower part of Kilauea's East Rift Zone. The implication is that geothermal energy resources are even more numerous in parts of the summit regions of Kilauea and Mauna Loa than in the area of the active PGV plant. This inference is supported by the findings of high-temperature steam vents and fumeroles (>100 °C) in Mauna Loa's summit caldera, and on Kilauea's upper and middle East Rift Zone (Casadevall and Hazlett, 1979, 1983), but a lack of such venting on the lower East Rift Zone around the PGV plant. Probabilities are less than those near PGV at select locations on or near the older shield volcanoes of Mauna Kea, Haleakala, West Maui, and Lanai; relatively low on south and west Oahu; and minimal on Kauai.

Whereas the resource potential is highest on the active volcanos of Hawaii Island, there are problems with pursuing development at those locations including elevated risks of natural hazards, the difficulties of permitting in national park lands, the sparsity of utility infrastructure, as well as the remoteness from large populations that would use the power generated. Furthermore, there are high costs and significant engineering challenges involved in transporting power between the islands to meet the large differences in island populations and energy demand. This means that areas with even moderate to low probabilities on the other islands should be considered for further investigation. Ultimately, the decisions about where to pursue further exploration should consider the results of the current analysis as well as issues pertaining to the practical, economic, as well as societal viability of geothermal power development. These aspects are addressed in the third paper of this series (Lautze et al., 2016b).

Acknowledgements

This project was funded by U.S. Department of Energy's Geothermal Technologies Program award number DE-EE6729. We appreciate the generous input provided by John Sinton, James Foster, Stephen Martel, and Ormat geologists, and thank B.S. student Hannah Schuchmann as well as Mahany Lindquist for their enthusiastic participation. Valuable reviews were provided by John Shervais, an anonymous reviewer, and Associate Editor, David Bruhn.

References

Bianco, T.A., Ito, G., Becker, J.M., Garcia, M.O., 2005. Secondary Hawaiian volcanism formed by flexural arch decompression. Geochem. Geophys. Geosys. 6, Q08009, http://dx.doi.org/10.1029/2004GC000860.

Bonham-Carter, G.F., Agterberg, F.P., Write, D.F., 1989. Weights of evidence modeling: a new approach to mapping mineral potential. In: Agterberg, F.P., Bonham-Carter, G.F. (Eds.), Statistical Applications in the Earth Sciences. Geol. Survey, Canada, pp. 171–183.

Bonham-Carter, G.F., 1994. Geographic Information Systems for Geoscientists: Modeling with GIS. Permagon Press, Ontario, Canada.

Box, G.E.P., Draper, N.R., 1987. Empirical Model-Building and Response Surfaces. Wiley, pp. 424.

Brooks, B.A., Foster, J.H., Bevis, M., Wolfe, C., Behn, M., 2006. Periodic slow earthquakes on the flank of Kilauea volcano Hawai'i. Earth Planet. Sci. Lett. 246, 207–216.

Carranza, E.J.M., Hale, M., 2003. Logistic regression for geologically constrained mapping of gold potenial Baguio District, Philippines. Explor. Min. Geol. 10, 165–175.

Casadevall, T.J., Hazlett, R.W., 1979. Inventory of active steam vents and fumaroles on Hawaiian volcanoes. In: Decker, R.W., Drake, C., Eaton, G.P., Helsey, C. (Eds.), Hawaii Symposium on Intraplate Volcanism and Submarine Volcanism. U. S. Geological Survey, Hawaiian Volcano Observatory, Hawaii National Park, HI USA.

Casadevall, T.J., Hazlett, R.W., 1983. Thermal areas on kilauea and mauna Loa volcanoes Hawaii. J. Volcanol. Geotherm. Res. 16, 173–188.

Coolbaugh, M., Bedell, R.L., 2006. A simplification of weights of evidence using a density function, fuzzy distributions, and geothermal systems. In: Harris, J.R. (Ed.), GIS for the Earth Sciences. Geol. Assoc., Canada, pp. 115–130.

Coolbaugh, M.F., Taranik, J.V., Raines, G.L., Shevenell, L.A., Sawatsky, G.L., Bedell, R., Minor, T.B., 2002. A geothermal GIS for Nevada: defining regional controls and favorable exploration terrains for extensional geothermal systems. Geotherm. Res. Counc. Trans. 26, 485–490.

Coolbaugh, M., Zehner, R., Kreemer, C., Blackwell, D., Oppliger, G., 2005. A map of geothermal potential for the Great Basin USA: recognition of multiple geothermal environments. Geotherm. Res. Counc. Trans. 29, 223–227.

Coolbaugh, M., Raines, G.L., Zehner, R., 2007. Assessment of exploration bias in data-driven predictive models and the estimation of undiscovered resources. Nat. Resour. Res. 16, 199–207.

Cox, M.E., Thomas, D.M., 1979. Cl/Mg ratio of Hawaiian groundwaters as a regional geothermal indicator. Geotherm. Res. Counc. Trans. 3, 145–148.

Domingos, P., Pazzani, M., 1997. On the optimality of the simple Bayesian classifier under zero-one loss. Mach. Learn. 29, 103–130.

Engott, J.A., Johnson, A.G., Bassiouni, M., Isuka, S.K., 2015. Spatially Distributed Groundwater Recharge for 2010 Land Cover Estimated Using a Water-budget Model for the Island of O'ahu, Hawai'i. U. S. Geol. Surv. Invest. Rep, 2015-5010, 49 p. http://dx.doi.org/10.3133/sir20155010.

Flinders, A., Ito, G., Garcia, M.O., Sinton, J.M., Kauahikaua, J., Taylor, B., 2013. Intrusive dike complexes, cumulate cores, and extrusive growth of Hawaiian volcanoes. Geophys. Res. Lett. 40, 3367–3373, http://dx.doi.org/10.1002/grl.50633.

Ingebritsen, S.E., Manning, C.E., 2010. Permeability of the continental crust: dynamic variations inferred from seismicity and metamorphism. Geofluids 10, 193–205.

Johnson, A.G., Engott, J.A., Bassiouni, M., 2014. Spatially Distributed Groundwater Recharge Estimated Using a Water-budget Model for the Island of Maui, Hawai'i, 1978–2007. U. S. Geol. Surv. Invest. Rep, 2014-5168, 53 p. http://dx.doi.org/10.3133/sir20145168.

Lautze, N., Thomas, D., Hinz, N., Ito, G., Frazer, N., Waller, D., 2016a. Play fairway analysis of geothermal resources across the state of Hawaii: 1. Geological, geophysical, and geochemical datasets. Geothermics, submitted for publication.

Lautze, N., Thomas, D., Waller, D., Frazer, N., Hinz, N., Ito, G., 2016b. Play Fairway Analysis of Geothermal Resources across the State of Hawaii: 3: Use of development viability criterion to prioritize future exploration targets. Geothermics, submitted for publication.

MCullah, P., Nelder, J.A., 1983. Generalized Linear Models. Chapman & Hall, New York.
Martel, S.J., Langley, J.S., 2006. Propagation of normal faults to the surface in basalt Koae fault system, Hawaii. J. Struct. Geol. 28, 2123–2143.
Matoza, R.S., Shearer, P.M., Lin, G., Wolfe, C.J., Okubo, P.G., 2013. Systematic relocation of seismicity on Hawaii Island from 1992 to 2009 using waveform cross correlation and cluster analysis. J. Geophys. Res. 118, 2275–2288, http://dx.doi.org/10.1002/jgrb.50189.
Noorollahi, Y., Itoi, R., Fujii, H., Tanaka, T., 2008. GIS integration model for geothermal exploration and well siting. Geothermics 37, 107–131.
O'Hagan, A., Buck, C.E., Daneshkhah, A., Eiser, J.R., Garthwaite, P.H., Jenkinson, D.J., Oakley, J.E., Rakow, T., 2006. Uncertain Judgements: Eliciting Expert Probabilities. Wiley, United Kingdom.
O'Leary, R.A., Choy, S.L., Murray, J.V., Kynn, M., Denham, R., Martin, T.G., Mengersen, K., 2009. Comparison of three expert elicitation methods for logistic regression on predicting the presence of the threatened brush-tailed rock-wallaby *Petrogale penicillata*. Environmetrics 20, 379–398.
Okubo, P.G., Benz, H.M., Chouet, B.A., 1997. Imaging the crustal magma sources beneath Mauna Loa and Kilaeuea volcanoes, Hawaii. Geology 25, 867–870.
Pierce, H.A., Thomas, D.M., 2009. Magnetotelluric and Audiomagnetotelluric Groundwater Survey Along the Humu'ula Portion of Saddle Road near and Around Pohakuloa Training Area, Hawaii. USGS Open-File Rep (2009-1135).
Pollard, D.D., Segall, P., 1987. Theoretical displacements and stresses near fractures in rock: with applications to faults, joints, veins, dikes, and solution surfaces. In: Atkinson, B.K. (Ed.), Fracture Mechanics of Rock. Academic Press, New York, pp. 277–349.
Porwal, A.K., Kreuzer, O.P., 2010. Introduction to the Special Issue: mineral prospectivity analysis and quantitative resource estimation. Ore Geol. Rev. 38, 121–127.
Porwal, A., Carranza, E.J.M., Hale, M., 2006. Bayesian network classifiers for mineral potential mapping. Comput. Geosci. 32, 1–16.
Prol-Ledesma, R.M., 2000. Evaluation of reconnaissance results in geothermal exploration using GIS. Geothermics 29, 83–103.
Rotzoll, K., El-Kadi, A.I., 2007. Numerical Ground-Water Flow Simulation for Red Hill Fuel Storage Facilities, NAVFAC Pacific, Oahu, Hawaii, Prepared for TEC, Inc. by the Water Resources Research Center, Univ. of Hawaii, Honolulu, 83 p.
Siler, D.L., Faulds, J.E., Mayhew, B., McNamara, D.D., 2016. Analysis of the favorability for geothermal fluid flow in 3D: Astor Pass geothermal prospect, Great Basin, northwestern Nevada, USA. Geothermics 60, 1–12.
Sinton, J.M., Eason, D.E., Tardona, M., Pyle, D., van der Zander, I., Guillou, H., Clague, D.A., Mahoney, J.J., 2014. Ka'ena Volcano—a precursor volcano of the island of O'ahu, Hawai'i. Geol. Soc. Am. Bull. 126, 1219–1244 http://dx.doi.org/10.1130/B30936.1.
Sommerfeld, A., 1964. Partial Differential Equations in Physics. Academic Press, New York.
Tüfekçi, N., Lütfi Süzen, M., Nilgün, G., 2010. GIS based geothermal potential assessment: a case study from Western Anatolia, Turkey. Energy 35, 246–261.
Thomas, D.M., 1985. Geothermal Resources Assessment in Hawaii: Final Report. Hawaii Institute for Geophysics Technical Report (HIG-8502, 115 p).
Tilling, R., Rhodes, J.M., Sparks, J.W., Lockwood, J.P., Lipman, P.W., 1987. Disruption of the Mauna Loa magma system by the 1868 Hawaii earthquake: geochemical evidence. Science 235, 196–199.
Trumpy, E., Donato, A., Gianelli, G., Gola, G., Misissale, A., Montanari, D., Santilano, A., Manzella, A., 2015. Data integration and favourability maps for exploring geothermalsystems in Sicily, southern Italy. Geothermics 56.
Turcotte, D.L., Schubert, G., 2002. Geodynamics, second edition. Cambridge University Press, New York, pp. 456.
Wessel, P., Smith, W.H.F., Scharroo, R., Luis, J.F., Wobbe, W., 2013. Generic mapping tools: improved version released. EOS Trans. AGU 94, 409–410.
Whittier, R.B., El-Kadi, A.I., 2014. Human Health and Environmental Risk Ranking of On-Site Sewage Disposal Systems for the Hawaiian Islands of Kauai, Molokai, Maui, and Hawaii – Final, Prepared for the Hawaii Dept. of Health by University of Hawaii at Manoa, Dept. of Geology and Geophysics, 252 p.
Yousefi, H., Noorollahi, Y., Ehara, S., Itoi, R., Yousefi, A., Fujimitsu, Y., Nishijima, J., Sasaki, K., 2010. Developing the geothermal resources map of Iran. Geothermics 39, 140–151.